Research Square

Preprints are preliminary reports that have not undergone peer review.
They should not be considered conclusive, used to inform clinical practice,
or referenced by the media as validated information.

Damage Evolution and Critical Failure Regions in Dry-Towpreg-Wound 70 MPa Type IV Hydrogen Vessels

Xinyue Leng
North China Institute of Aerospace Engineering
Zhixu Zhang
Tianjin Towpreg Technology Co
Zhipeng Xu
North China Institute of Aerospace Engineering
Jingyu Zhao
North China Institute of Aerospace Engineering
Yonghao Li
North China Institute of Aerospace Engineering
Bo Yang
North China Institute of Aerospace Engineering
Yilei Yue
North China Institute of Aerospace Engineering
Jiazhong Xu
North China Institute of Aerospace Engineering
Song Lin
linsong28@nciae.edu.cn
North China Institute of Aerospace Engineering
Linan Xu
North China Institute of Aerospace Engineering

Research Article

Keywords: Type IV hydrogen vessel, dry towpreg winding, matrix damage, fiber damage, progressive failure, critical failure region

Posted Date: September 8th, 2026

DOI: https://doi.org/10.21203/rs.3.rs-10520024/v1

License: This work is licensed under a Creative Commons Attribution 4.0 International License.
Read Full License

Additional Declarations: No competing interests reported.

Damage Evolution and Critical Failure Regions in Dry-Towpreg-Wound 70 MPa Type IV Hydrogen Vessels

Xinyue Leng[a] ,Zhixu Zhang [c], Zhipeng Xu [a], Jingyu Zhao[a], Yonghao Li [a], Bo Yang [a], Yilei Yue [a], Jiazhong Xu [b], Song Lin [*, a], Linan Xu [**,a]

[a] School of Materials Science and Engineering, North China Institute of Aerospace Engineering, Langfang 065000, PR China.

[b] Institute of Automation, Harbin University of Science and Technology, Harbin 150000, PR China.

[c] Tianjin Towpreg Technology Co., Ltd., Tianjin 300000, PR China

*Corresponding Author at: School of Materials Science and Engineering, North China Institute of Aerospace Engineering, Langfang 065000, PR China.

**Corresponding Author.

E-mail addresses: linsong28@nciae.edu.cn (S. Lin), xulinan1232@nciae.edu.cn (L. Xu)

Abstract: This study investigated the evolution and spatial localization of pressure-induced damage in dry-towpreg-wound 70 MPa Type IV composite overwrapped pressure vessels (COPVs) for hydrogen storage. A process-based, layer-wise finite element model was established to represent the spatially varying winding angle and thickness build-up in the polar, dome, and dome–cylinder transition regions. Progressive damage was described using the Hashin failure criterion and mode-dependent stiffness degradation implemented in ABAQUS through a USDFLD subroutine. The model was evaluated using hydrostatic burst tests on three full-scale vessels. Matrix tensile damage first appeared at approximately 32 MPa near the polar boss and dome–cylinder transition, where geometric discontinuity and stiffness mismatch produced local stress concentrations. With increasing pressure, matrix tensile damage propagated into the cylindrical section, while fiber tensile damage developed at higher pressure levels and formed extensive damage regions near the final numerical stage. Compressive damage remained limited throughout the loading process. A marked nonlinear change in the pressure–displacement response occurred at approximately 165 MPa, indicating progressive stiffness degradation. Numerical loss of convergence occurred at 189.0 MPa and was adopted as the predicted burst pressure. The measured mean burst pressure was 181.7 ± 2.7 MPa, corresponding to a relative deviation of 4.0%. The predicted critical region at the dome–cylinder transition was consistent with the severe post-burst fragmentation involving the transition and adjacent cylindrical section. These findings establish a physically grounded link between process-induced geometric heterogeneity, progressive damage evolution, and failure localization, providing a mechanistic basis for critical-region-oriented design of high-pressure Type IV hydrogen vessels.

Keywords: Type IV hydrogen vessel; dry towpreg winding; matrix damage; fiber damage; progressive failure; critical failure region

1. Introduction

Hydrogen is increasingly considered an important energy carrier for low-carbon transportation and energy systems because of its high gravimetric energy density and clean conversion characteristics [1].

However, its low volumetric density under ambient conditions requires compression to high pressures for practical onboard storage [2]. Stationary hydrogen storage can also combine gaseous and solid-state storage routes to balance storage capacity and delivery performance [3]. Type IV composite overwrapped pressure vessels (COPVs), which consist of a polymer liner, metallic bosses, and a carbon-fiber-reinforced polymer overwrap, are widely used for 70 MPa hydrogen storage because of their low structural mass, corrosion resistance, and fatigue performance [4]. These vessels store substantial elastic strain energy under service conditions. International standards therefore require adequate burst-pressure margins relative to the nominal working pressure [5,6]. Reliable structural assessment must address not only the ultimate burst pressure but also the evolution and spatial localization of damage before burst.

The failure response of a Type IV COPV is controlled by the combined effects of material anisotropy, winding architecture, geometric discontinuity, and load redistribution after local damage. Preliminary sizing often relies on membrane or netting-based assumptions, whereas detailed numerical analyses account for variable dome contours and local stress transfer [7]. Such simplified assumptions are useful for initial sizing but are insufficient for resolving the local mechanical response of thick-walled 70 MPa vessels [8-10]. High stress gradients can develop near the polar boss and dome–cylinder transition because of curvature changes, multi-material interfaces, and stiffness mismatch. These local effects can initiate matrix damage before the fiber-dominated load-bearing capacity is significantly reduced. Membrane-based analytical methods cannot fully capture this progressive and spatially nonuniform response.

Finite element analysis provides a practical means of resolving the local stress and damage fields in composite pressure vessels [11]. However, the reliability of the prediction depends strongly on the selected failure description. Several strength criteria and failure envelopes have been proposed and assessed for composite laminates [12-15]. Maximum stress, maximum strain, Tsai-Wu-type, and related mode-independent criteria can identify failure onset, but they generally do not explicitly distinguish matrix tensile damage, matrix compressive damage, fiber tensile damage, and fiber compressive damage. First-ply

failure is also unsuitable as a direct burst criterion because a composite laminate can continue to carry load after initial matrix cracking through stress redistribution among the remaining layers [16-18]. Progressive damage analysis is therefore required to update the material stiffness after each failure mode is activated and to trace the transition from localized matrix damage to extensive fiber-related damage and structural stiffness loss. Experimental and numerical studies of CFRP laminates have likewise shown that progressive damage models can reproduce the transition from matrix-dominated damage to fiber fracture and the associated nonlinear load–displacement response [19].

The geometric representation of the wound overwrap is another important factor in damage prediction. Filament winding produces continuous spatial variations in helical winding angle and local thickness, particularly in the polar, dome, and dome–cylinder transition regions [20,21]. Tow turnaround, overlap, and redistribution cause local thickness build-up, while the fiber direction changes continuously along the dome profile. These variations affect the local stiffness, load-transfer path, and stress concentration. Prior studies have represented these effects through progressive vessel models, continuous transition-line patterns, ply-overlap optimization, and dome-thickness prediction methods [22-25]. Even so, geometric idealization can obscure local damage-sensitive regions and alter the predicted damage sequence. A process-based, layer-wise representation is therefore needed to examine how winding-induced geometric heterogeneity contributes to damage initiation and failure localization. Recent studies have further shown that dome geometry, winding-layer thickness, polar ratio, and boss dimensions can significantly affect the stress distribution of Type IV vessels, with peak stresses frequently occurring near the dome–cylinder transition [26].

The manufacturing route also influences the consistency of the wound architecture. Dry towpreg winding uses carbon-fiber tows that are impregnated before placement, rather than fibers impregnated in a resin bath during winding. This process can improve the control of matrix content, fiber-volume fraction, tow compaction, and layer repeatability in thick composite overwraps [27]. However, dry-towpreg-wound

structures can still contain process-related variations, including local voids and nonuniform consolidation [28]. The mechanical response of these vessels is therefore governed by both the designed winding architecture and manufacturing-induced variability. Recent computational–experimental work has also shown that idealized Type IV vessel models may diverge from as-built performance when material–process compatibility, winding tension, process-induced defects, and equipment constraints are neglected [29]. At the material scale, variations in fiber-volume fraction and fiber clustering can modify local extreme stress fields and the propensity for matrix-dominated damage initiation [30]. Existing studies have not sufficiently clarified the relationship among process-consistent layer-wise geometry, mode-dependent progressive damage, and critical failure-region formation in full-scale dry-towpreg-wound 70 MPa Type IV vessels.

This study investigates the pressure-dependent damage evolution and failure localization of dry-towpreg-wound 70 MPa Type IV hydrogen vessels. A process-based, layer-wise finite element model is established using helical winding equations to represent the spatial variations in winding angle and thickness within the polar, dome, and dome–cylinder transition regions. The Hashin failure criterion and mode-dependent stiffness degradation are implemented in ABAQUS through a USDFLD subroutine to distinguish the principal matrix and fiber damage modes during internal pressurization. Hydrostatic burst tests are conducted on three full-scale vessels to evaluate the predicted burst pressure and critical damage region. The study focuses on three linked questions: where damage first develops, how matrix- and fiber-related damage evolves with increasing pressure, and why the dome–cylinder transition becomes a critical region near the final failure stage. By connecting winding-induced geometric heterogeneity with damage redistribution and failure localization, this work provides a mechanistic basis for critical-region-oriented assessment and subsequent structural design of high-pressure Type IV hydrogen vessels.

2. Experimental

2.1. Materials and Equipment

Materials: The composite overwrap was fabricated using a carbon-fiber/epoxy dry towpreg system. The

matrix consisted of a TDE-85/E-51 epoxy blend with a weight ratio of 7:3, and an amine-based curing agent (E100, Jining Baichuan Chemical Co., Ltd.) was used as the hardener during prepreg tow preparation. The reinforcement was SYT49S-12K carbon fiber supplied by Zhongfu Shenying Carbon Fiber Co., Ltd.

The vessel incorporated a 23 L plastic liner and a valve seat fabricated from 6061-T6 aluminum alloy (Southwest Aluminum (Group) Co., Ltd.). PA6 polymer (PA6-I, an imported grade processed domestically) was used as the liner material. The specific dimensions of the vessel are shown in Figure 1.

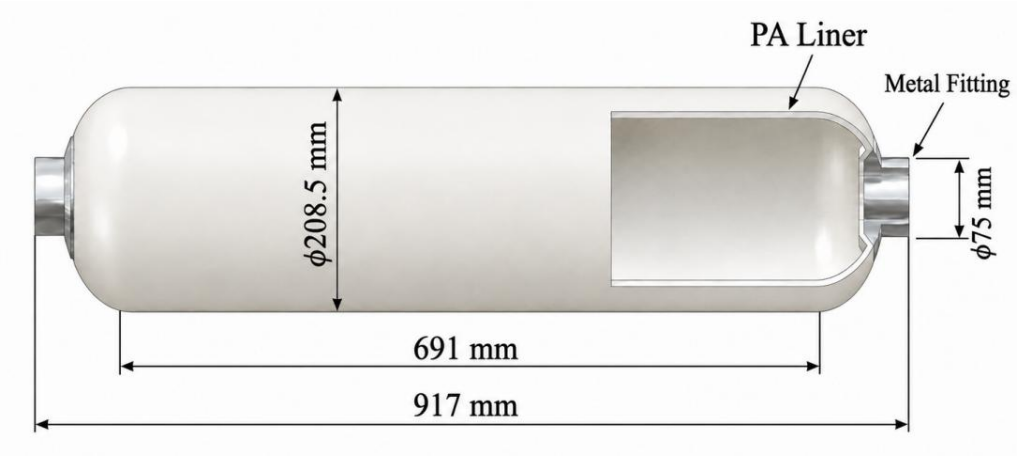


Fig. 1 Dimensional drawing of the plastic liner

Equipment: Dry towpreg winding was performed using a six-axis collaborative winding machine (FWA-1/6/1). Curing was carried out in a trolley-type curing oven (ITVU-1/4). Burst tests were conducted with a hydraulic burst testing device (SY-IV/WC, Jiangsu Zhonghong Machinery Manufacturing Co., Ltd.).

2.2. Fabrication of Type IV Composite Pressure Vessels

The Type IV composite pressure vessels were fabricated using a dry towpreg winding process. A representative vessel during winding is shown in Figure 2. Unlike conventional wet filament winding, in which dry carbon fibers are impregnated in a resin bath during winding, the carbon-fiber tow used in this study was pre-impregnated with the epoxy matrix system before winding. During vessel fabrication, the towpreg was continuously wound onto the PA6 liner under controlled tension and trajectory conditions, without additional in-situ matrix impregnation. This process was adopted to improve the consistency of matrix content, fiber-volume fraction, tow placement, and layer repeatability during the fabrication of thick-walled 70 MPa Type IV vessels.

The total thickness of the fiber-wound composite overwrap was approximately 25 mm, with the winding sequence alternating between helical and hoop layers. The helical and hoop winding angles were designed according to the layup scheme listed in Table 1. In the cylindrical section, hoop layers were mainly used to resist circumferential stress, whereas helical layers provided load transfer between the cylindrical section and the dome regions. In the dome region, the helical winding angle and local layer thickness varied spatially because of the winding trajectory and tow redistribution, which provided the geometric basis for the layer-wise reconstruction described in Section 3.1.

Table 1 Winding sequence and layer architecture

Winding angle
±89.0° /±34.0° /±55.0° /±89.0° /±13.5° /±41.0° /±32.9° /±89.0° /±16.6° /±89.0° /±29.8° /±25.1° /±89.0° /±16.0° /±89.0° /±24.0° /89.0° /±15.4° /±89.0° /±19.2° /±14.0° /±14.0° /±89.0°

Each nominal composite layer had a thickness of 0.22 mm. After winding, the vessels were cured in an oven using a rotational curing technique to maintain geometric stability and reduce matrix redistribution during the thermal cycle. The curing schedule consisted of holding the vessels at 70 °C for 1 h and then at 120 °C for 3 h, with a controlled heating rate of 1 °C/min. Three composite pressure vessels, labeled 1# through 3#, were fabricated for subsequent validation by hydrostatic burst testing.

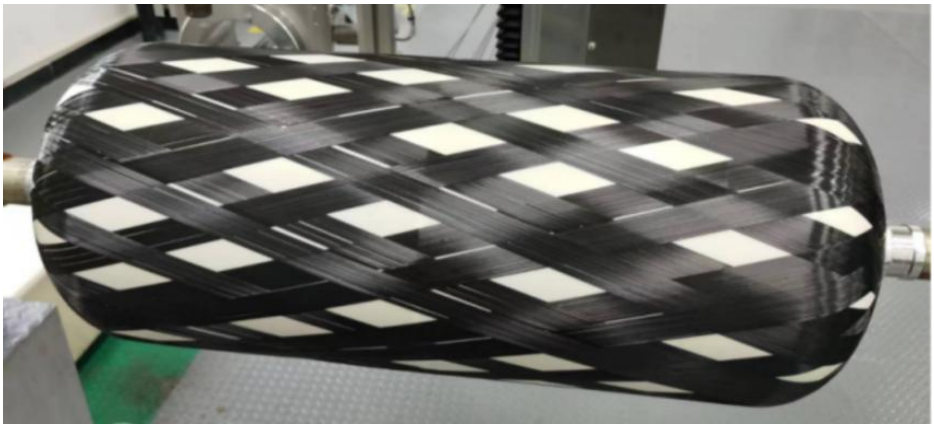


Fig. 2 Representative winding pattern of the dry-towpreg-wound 70 MPa Type IV vessel

2.3. Hydrostatic Burst Testing

Hydrostatic burst tests were conducted on the wound composite pressure vessels in accordance with the Group Standard T/CATSI 02007-2020, Fully Wrapped Carbon Fiber Composite Pressure Vessels with Plastic Liners for Compressed Hydrogen Gas in Vehicles. The recorded data included the burst pressures, burst-pressure curves, and photographs documenting the final burst modes.

3. Finite Element Analysis of Type IV Composite Pressure Vessels

3.1. Finite Element Modeling of Composite Pressure Vessels

A finite element model was developed for the pressure vessel in Abaqus using the following equations [31].

Helical Wind Angle:

$$\theta(R) = \sin^{-1}(R_0/R) - \delta[(R - R_0)/(R_{tl} - R_0)]^{\mathrm{n}} \tag{1.1}$$

$$\delta = \theta_{tl} - \sin^{-1}(R_0/R_{tl}) \tag{1.2}$$

Here, R is the radial distance from the centerline to a point in the layer, R_0 is the radial distance from the centerline to the turnaround point, R_{tl} is the radius at the dome–cylinder tangent line, δ denotes the angular deviation from the frictionless winding angle.

Helical Thickness Buildup:

$$t(r) = r_{tl} \cdot t_{tl} \cdot \cos(\theta_{tl})/\cos(\theta_r) \cdot \{r + 2 \cdot BW \cdot [(r_{tl} - r)/(r_{tl} - r_0)]^4\} \tag{1.3}$$

Here, t_{tl} is the thickness at the tangent line, θtl is the winding angle at the tangent line, θr is the winding angle at radius r, r_{tl} is the radius at the dome–cylinder tangent line, r0 is the radius at the helical turnaround point, r is the radius at a given point on the dome, and BW is the helical-band width.

As shown in Figure 3, a three-dimensional circumferential sector model with an angular extent of 3° was constructed, including the metal fitting, PA6 liner, and composite overwrap. Using the aforementioned formulations, the winding process was simulated to define the helical layers in the dome regions with spatially varying angles and thicknesses. The formulations, together with Abaqus and a compiled subroutine, enable the accurate construction of finite element models for composite pressure vessels.

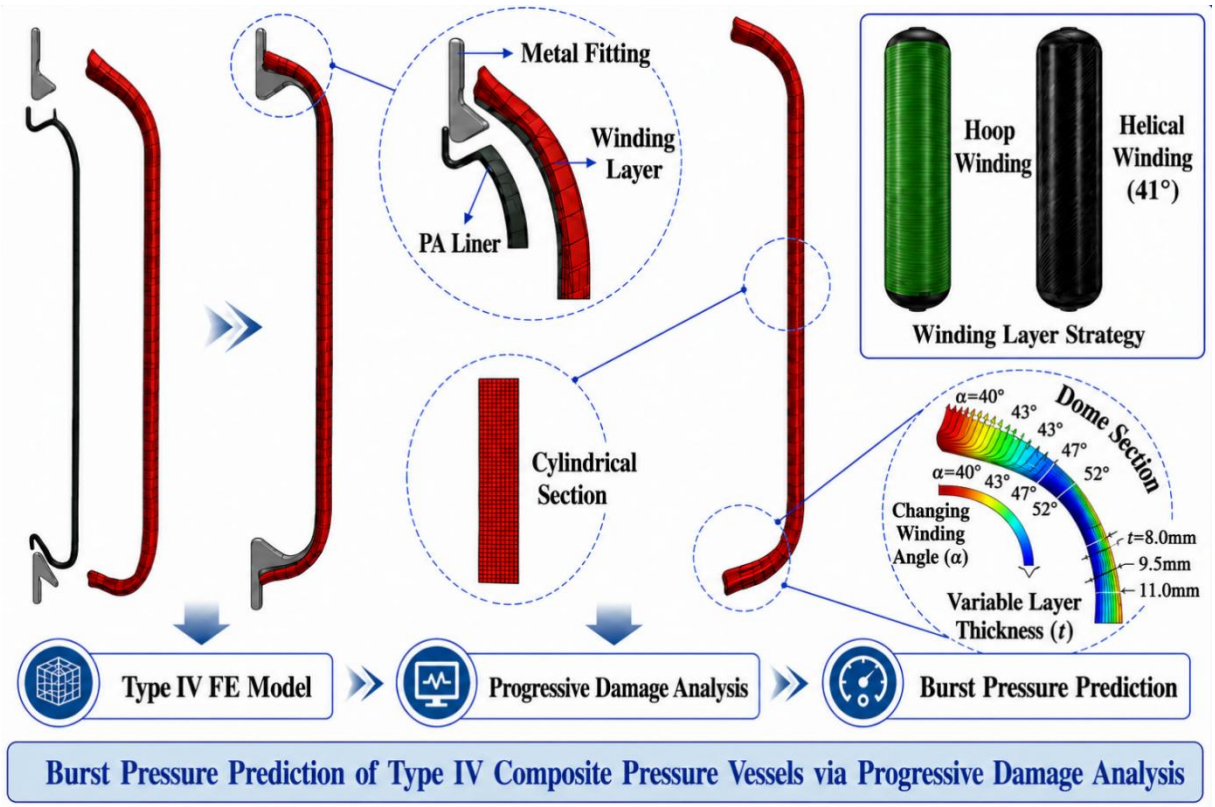


Fig. 3 Finite element model of the Type IV composite pressure vessel

Periodic rotational boundary conditions were applied to the model, and an internal pressure of 200 MPa was gradually introduced to the inner surface. Symmetric boundary conditions were imposed along the axial direction at the mid-plane of the composite layer. Tie constraints were applied at the interfaces between the metal fitting and PA6 liner, as well as between adjacent composite layers. The metal fitting and PA6 liner were discretized using C3D8R elements, while the composite layers were discretized using C3D8 elements. The tensile property curves of the metal fitting and PA6 liner are shown in Figures 4a and 4b, respectively, and were incorporated into the corresponding plasticity parameters within Abaqus.

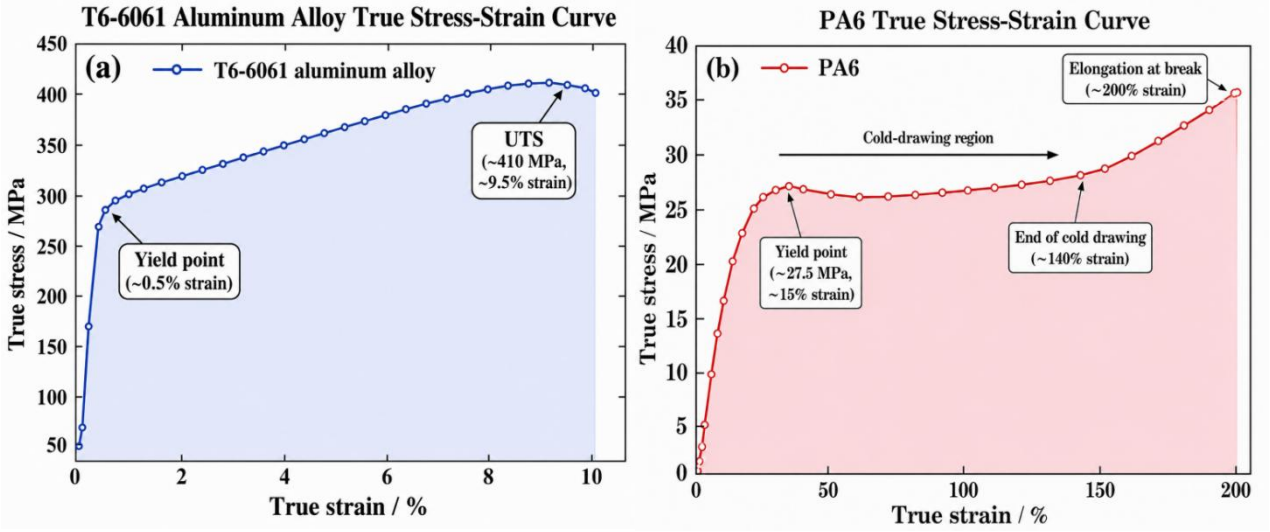


Fig. 4 True stress－strain curves of (a) 6061-T6 aluminum alloy and (b) PA6

The primary mechanical properties of the carbon-fiber composite are presented in Tables 2 and 3, whereas the key properties of the aluminum alloy and PA6 are listed in Table 4.

Table 2 Engineering constants used in the finite element analysis of the composite

Property	E_1 (GPa)	E_2 (GPa)	ν_{12}	ν_{23}	G_{12} (GPa)	G_{13} (GPa)	G_{23} (GPa)
Value	136	8.5	0.3	0.34	4.8	4.8	4.0

Table 3 Composite strength parameters used in the finite element analysis

Property	Xt (MPa)	Xc (MPa)	Yt (MPa)	Yc (MPa)	S_{12} (MPa)
Value	2400	1600	50	160	60

Table 4 Elastic properties of the aluminum alloy and PA6

Property	E (GPa)	ν
Aluminum alloy	73	0.34
PA6	2.0	0.38

3.2. Progressive Damage Analysis of Composites

3.2.1. Progressive Damage Analysis Procedure

This study focuses on progressive damage analysis (PDA) of the composite overwrap in Type IV pressure vessels subjected to internal pressure, with the aim of predicting burst pressure. The failure of composites typically progresses through a gradual sequence, beginning with matrix cracking, followed by delamination, and ultimately culminating in fiber fracture. Therefore, the selection of appropriate failure criteria is essential for accurate PDA.

This study applies the Hashin failure criterion for composites and implements a USDFLD subroutine in Abaqus based on this framework to perform the PDA. The analytical workflow is illustrated in Figure 5. The procedure begins by evaluating the stress state under internal pressure. The Hashin criterion is then employed to determine the onset of failure. If failure is identified, the corresponding material properties are reduced according to predefined degradation parameters, and the stiffness matrix is updated to account for the damage. The stresses are subsequently recalculated, and this iterative process is repeated until ultimate failure occurs.

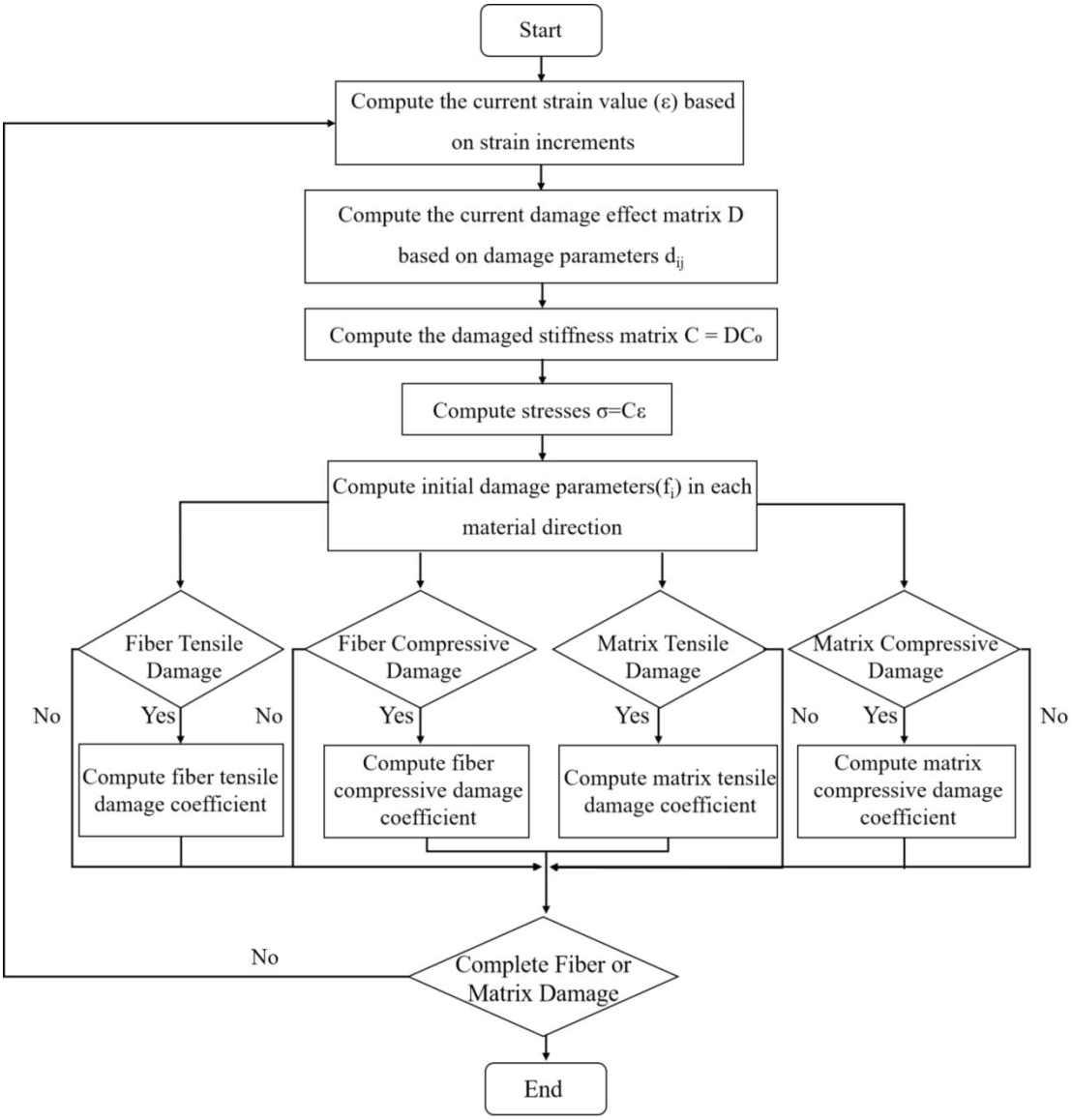


Fig. 5 Progressive damage analysis procedure based on the Hashin criterion

3.2.2. Hashin Failure Criterion and Material Degradation

The Hashin criterion was employed to analyze matrix damage, delamination, and fiber fracture in the

composite. The failure indices are expressed as follows [32]:

Fiber fracture failure:

Fiber tensile failure:

$$F_f^{t2}=(\sigma_{11}/X_t)^2+(\sigma_{12}/S_{12})^2+(\sigma_{13}/S_{13})^2\geq 1 \tag{2.1}$$

Fiber compressive failure:

$$F_f^{c2}=(\sigma_{11}/X_c)^2\geq 1 \tag{2.2}$$

Matrix failure:

Matrix tensile failure:

$$F_m^{t\ 2}=(\sigma_{23}/S_{23})^2+(\sigma_{12}/S_{12})^2+(\sigma_{13}/S_{13})^2-[(\sigma_{22}+\sigma_{23})/S_{23}]^2+[(\sigma_{22}+\sigma_{23})/S_{23}]^2\geq 1 \tag{2.3}$$

Matrix compressive failure:

$$F_m^{c\ 2}=(\sigma_{23}/S_{23})^2+(\sigma_{12}/S_{12})^2+(\sigma_{13}/S_{13})^2-[(\sigma_{22}+\sigma_{23})/S_{23}]^2+[(\sigma_{22}+\sigma_{23})/S_{23}]^2 +[(Y_c/2S_{23}-1)^2](\sigma_{22}+\sigma_{23}/Y_c)\geq 1 \tag{2.4}$$

Delamination failure:

$$F_d^2=(\sigma_{13}/S_{12})^2+(\sigma_{23}/S_{13})^2\geq 1 \tag{2.5}$$

When the stress state satisfies the corresponding failure criterion, the material properties of the damaged elements are reduced according to the selected stiffness degradation scheme. In this study, the Tan stiffness degradation criterion is adopted to describe the property reduction associated with fiber fracture, matrix cracking, and delamination. In Table 5, Md denotes the residual material property after damage initiation, while A denotes the corresponding undamaged property, such as an elastic modulus, Poisson's ratio, or shear modulus. The residual property is calculated by multiplying A by the mode-dependent degradation coefficient. The degradation relations for the different damage modes are summarized in Table 5.

Table 5 Residual property coefficients for different composite damage modes

Damage mode	Stiffness degradation relation
Fiber tensile fracture damage	M_d=0.07A , A∈ $\{E_1, \nu_{12}, \nu_{13}, G_{12}, G_{13}\}$
Fiber compressive fracture damage	M_d=0.14A , A∈ $\{E_1, \nu_{12}, \nu_{13}, G_{12}, G_{13}\}$
Matrix tensile damage	M_d=0.2A , A∈ $\{E_2, \nu_{12}, \nu_{23}, G_{12}, G_{13}\}$
Matrix compressive damage	M_d=0.4A , A∈ $\{E_2, \nu_{12}, \nu_{23}, G_{12}, G_{23}\}$
Delamination damage	M_d=0.2A , A∈ $\{E_3, \nu_{12}, \nu_{23}, G_{13}, G_{23}\}$

4. Results and Discussion

4.1. Progressive Damage Analysis of the Composite Pressure Vessel

Using the model described above, a PDA of the composite pressure vessel was performed by increasing the internal pressure incrementally until failure occurred. Throughout the process, the Hashin criterion was employed to evaluate matrix cracking and fiber fracture induced by internal pressure loading.

As shown in Figure 6, matrix tensile damage initiated at an internal pressure of 32 MPa. The damage was mainly concentrated near the boss opening and the dome–cylinder transition region. At this stage, the matrix tensile damage ratio was approximately 7.0%. When the pressure increased to the working pressure of 70 MPa, the damage ratio increased slightly to approximately 9.0%. The damage remained localized near the boss and the dome–cylinder transition region. A pronounced increase occurred at 105 MPa. The matrix tensile damage ratio reached approximately 48.0%, and the damaged region began to extend from the dome and transition regions into the cylindrical section. With further pressurization, the damage ratio increased to approximately 62.0% at 125 MPa and 70.0% at 140 MPa. These results indicate that matrix tensile damage progressively propagated through the composite overwrap before the predicted burst pressure was reached. At 189 MPa, the damage ratio reached approximately 79.2%, indicating widespread matrix tensile damage throughout the composite overwrap rather than complete matrix failure. Similar damage patterns were observed at the front and rear domes because of the nearly symmetric vessel geometry and winding configuration. The early damage near the boss and dome–cylinder transition region can be attributed to geometric discontinuity, curvature variation, and stiffness mismatch among the aluminum boss, PA6 liner,

and composite overwrap. These factors produce local stress concentrations and promote premature matrix cracking under internal pressure loading [33,34].

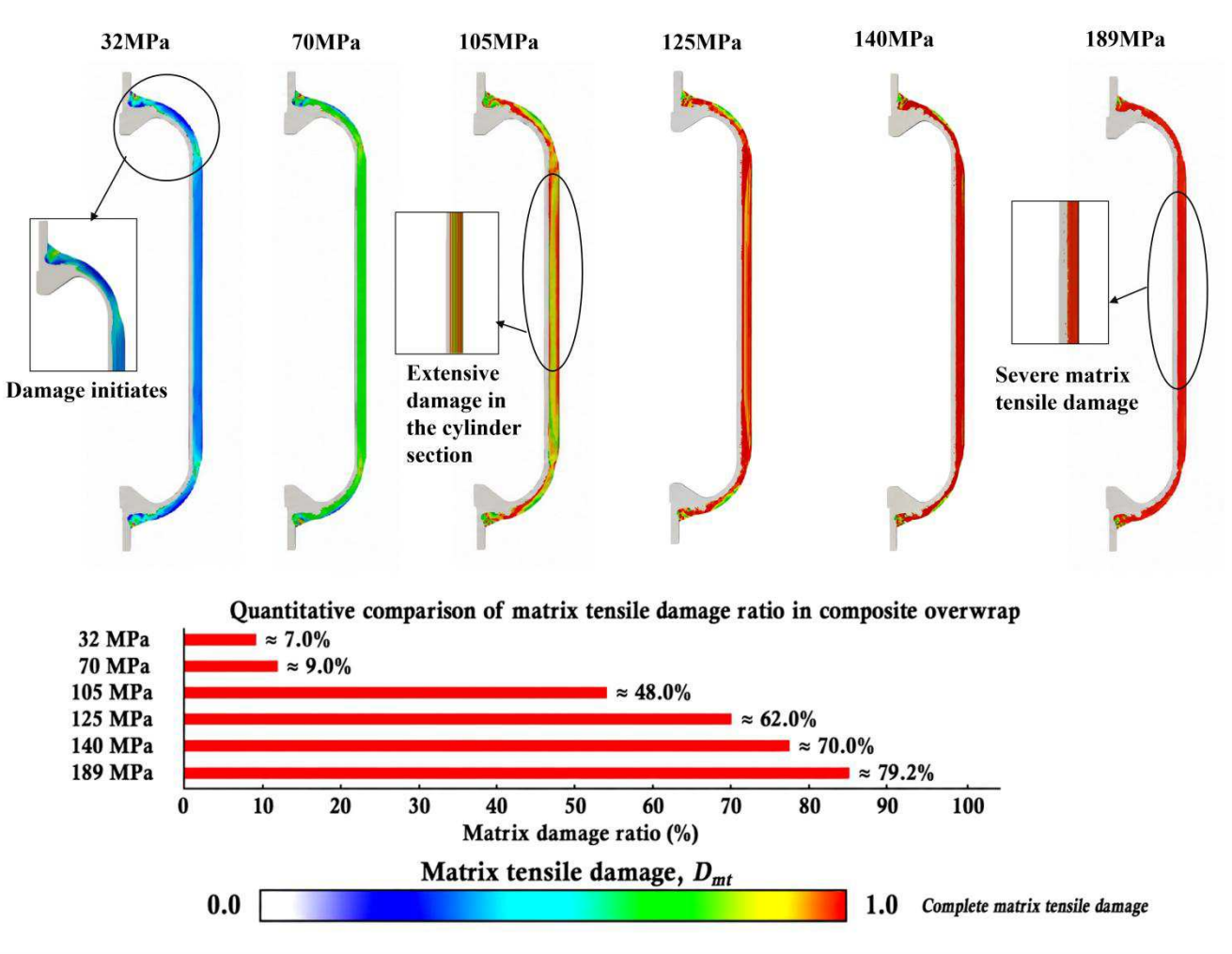


Fig. 6 Matrix tensile damage in the composite overwrap

As shown in Figure 7, matrix compressive damage remained limited at 189 MPa, with a damage ratio of approximately 2.1%. The damage was mainly localized near the nozzle connections and the cylinder–dome transition regions. Similar distributions were observed at both domes, indicating that matrix compressive damage played a secondary role in the burst process. Overall, the Type IV composite pressure vessel examined in this study predominantly exhibited matrix tensile damage under internal pressure. This damage initiated at the nozzle connection and the dome–cylinder transition region, subsequently propagating throughout the composite overwrap.

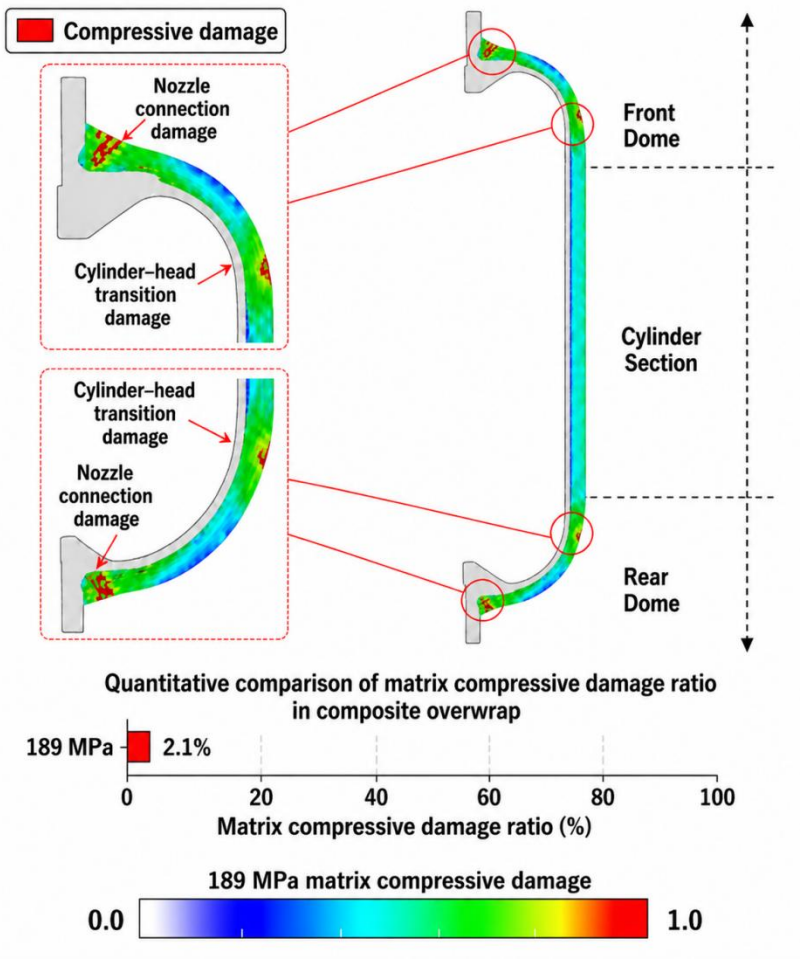


Fig. 7 Matrix compressive damage in the composite overwrap

In Type IV composite pressure vessels, the carbon-fiber overwrap serves as the primary load-bearing structure [35]. Therefore, fiber-dominated damage directly affects the pressure-bearing capacity of the vessel. As shown in Figure 8, fiber tensile damage remained limited at 73 and 93 MPa, with damage ratios of approximately 0.5% and 1.2%, respectively. The damage was mainly localized near the dome–cylinder transition regions. At 109 MPa, the fiber tensile damage ratio increased to approximately 14.4%, indicating pronounced damage propagation from the dome regions into the cylindrical section. Further pressurization to 146 MPa increased the damage ratio to approximately 32.5%, with high-damage regions extending over a larger portion of the composite overwrap. At 189 MPa, the fiber tensile damage ratio reached approximately 51.8%, and extensive damage was observed along the cylindrical section and the dome–cylinder transition regions. The damage near the rear dome transition was slightly more pronounced than that near the front dome, suggesting that this region may be more critical during the final failure stage. In contrast, Figure 8

shows that fiber compressive damage remained limited at 189 MPa, with a damaged volume fraction of approximately 0.2%. This tensile-dominated response is consistent with progressive failure studies of Type IV composite vessels, in which the composite overwrap governs damage evolution and burst behavior [36].

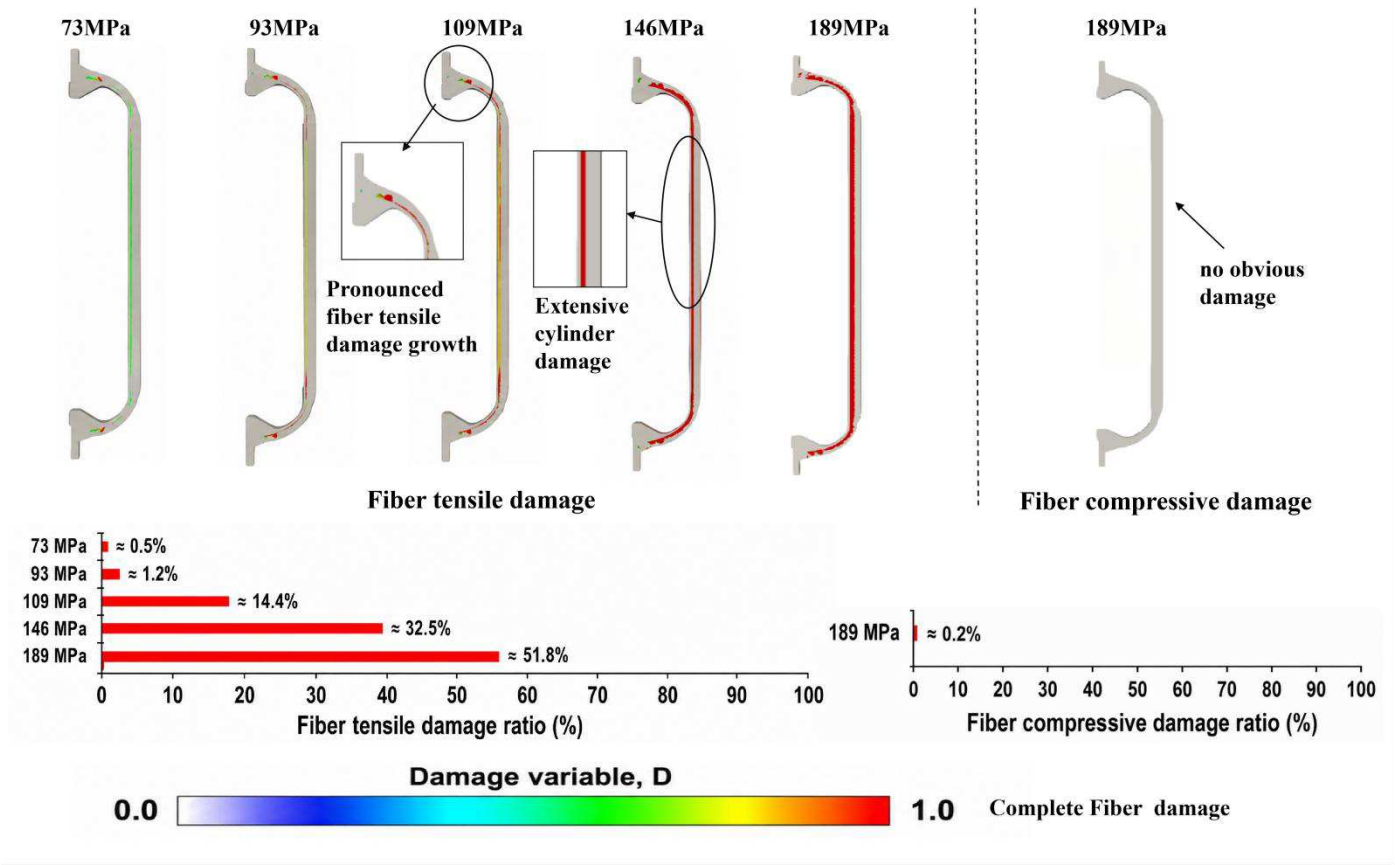


Fig. 8 Evolution and quantitative comparison of fiber damage

As illustrated in Figure 9, the damage distribution of the composite overwrap at an internal pressure of 189 MPa was evaluated based on the four Hashin failure modes. Among all failure modes, matrix tensile damage exhibited the highest damaged volume fraction, reaching approximately 79.2%, followed by fiber tensile damage with a damaged volume fraction of approximately 51.8%. In contrast, matrix compressive damage and fiber compressive damage remained limited, with damaged volume fractions of only 2.1% and 0.2%, respectively. These results indicate that tensile failure modes dominate the progressive damage evolution of the composite overwrap under internal pressure loading.

Comparison of Figures 6–8 further demonstrates that matrix tensile damage initiates earlier than fiber damage and gradually propagates with increasing pressure. This behavior is mainly attributed to the lower strength and stiffness of the polymer matrix compared with the carbon fibers, making the matrix more

susceptible to stress concentration-induced damage. Under internal pressure loading, the composite layers are primarily subjected to tensile stresses in the fiber and transverse directions, resulting in dominant matrix and fiber tensile damage rather than compressive failure.

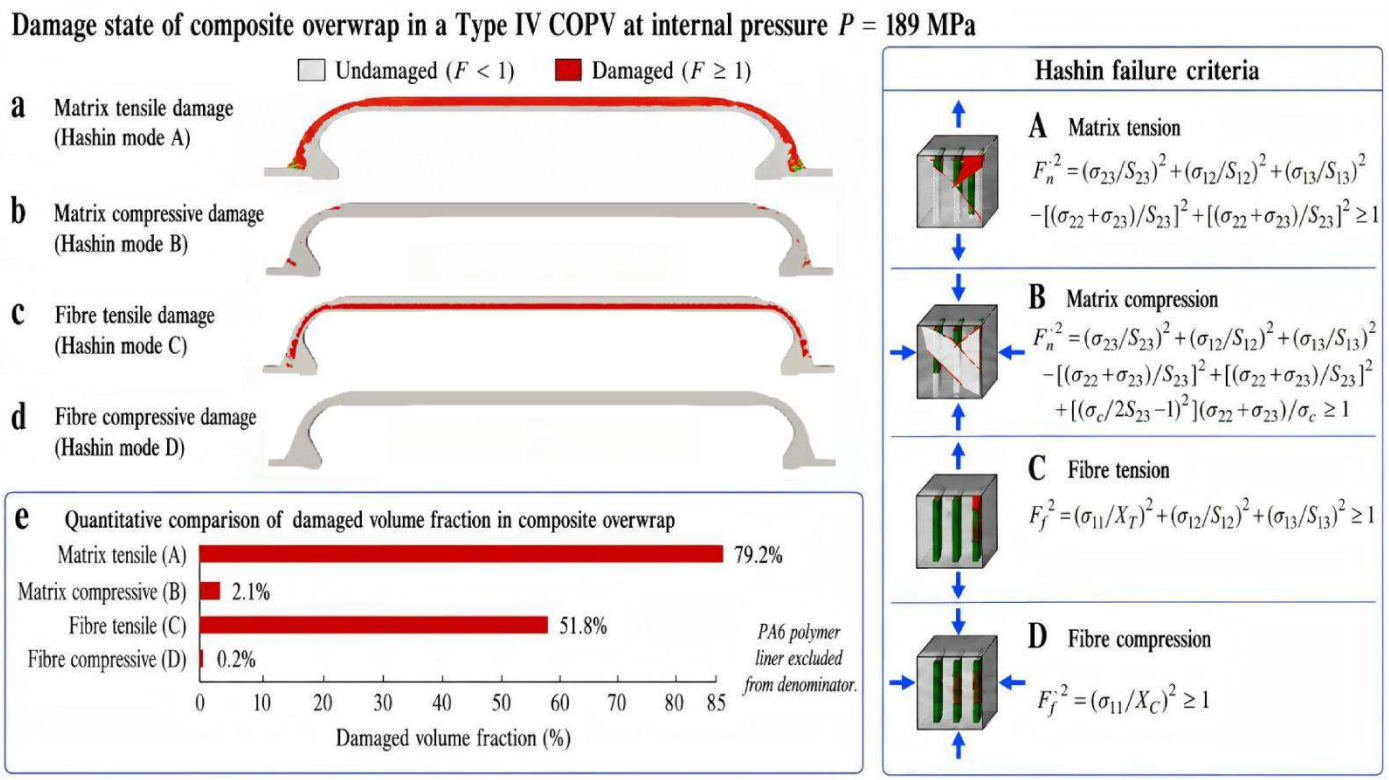


Fig. 9 Fiber and matrix damage in the composite overwrap at an internal pressure of 189 MPa

4.2. Burst-Pressure Prediction Based on Progressive Damage Analysis and Experimental Validation

The displacement responses of the dome–cylinder transition region, rear dome, and cylindrical section were examined. Figure 10 presents the pressure–displacement curves at the three representative locations, together with the displacement contour of the vessel.

During the initial pressurization stage, the displacement increases approximately linearly with internal pressure. This response indicates that the vessel remains predominantly in the elastic regime and that no pronounced stiffness degradation occurs. When the internal pressure approaches 165 MPa, the slopes of the displacement curves begin to increase. This nonlinear response indicates the onset and accumulation of progressive damage in the composite overwrap, including matrix cracking and fiber damage. The resulting reduction in structural stiffness causes the displacement to become increasingly sensitive to further pressure increments.

As the internal pressure increases from 165 to 189 MPa, the displacement growth becomes more pronounced in all three regions. The dome–cylinder transition region exhibits the largest displacement, followed by the rear dome, while the cylindrical section shows the lowest displacement. The displacement contour at 189 MPa further confirms that the maximum deformation is concentrated near the dome–cylinder transition region. This region is therefore identified as a critical location for damage accumulation and burst initiation.

At an internal pressure of 189 MPa, numerical divergence occurs because of extensive material degradation and rapid loss of structural stiffness. The simulation is terminated at this stage. Therefore, 189 MPa is taken as the predicted burst pressure of the composite pressure vessel.

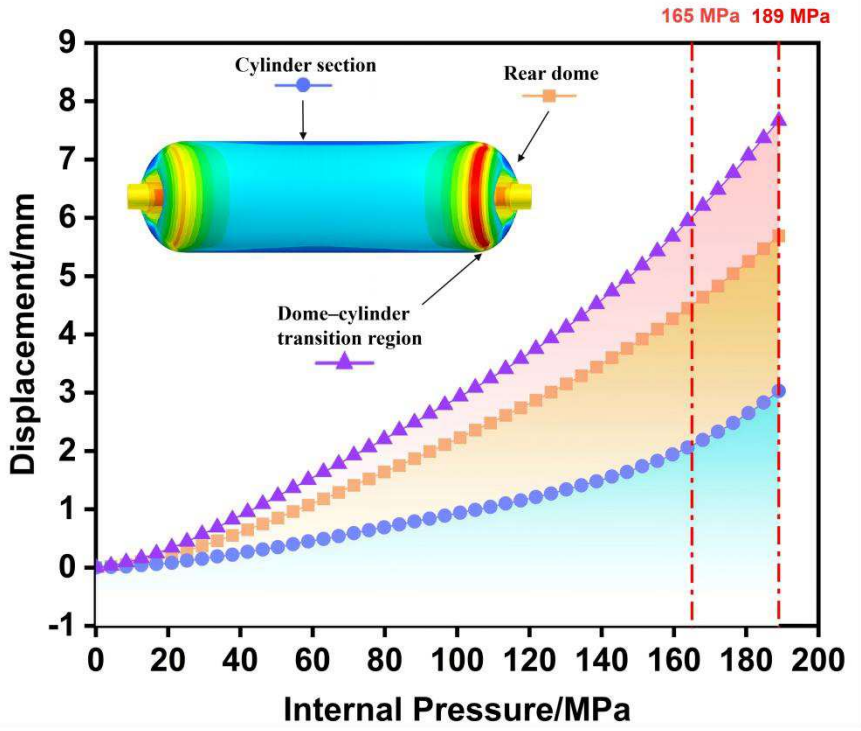


Fig. 10 Pressure–displacement responses at three representative locations and displacement contour at 189 MPa

Figure 11 presents the burst-pressure curves of composite pressure vessels 1#, 2#, and 3#. The curves show sharp drops at 184.7 MPa, 182.2 MPa, and 178.1 MPa, corresponding to the burst pressures of vessels 1#, 2#, and 3#, respectively.

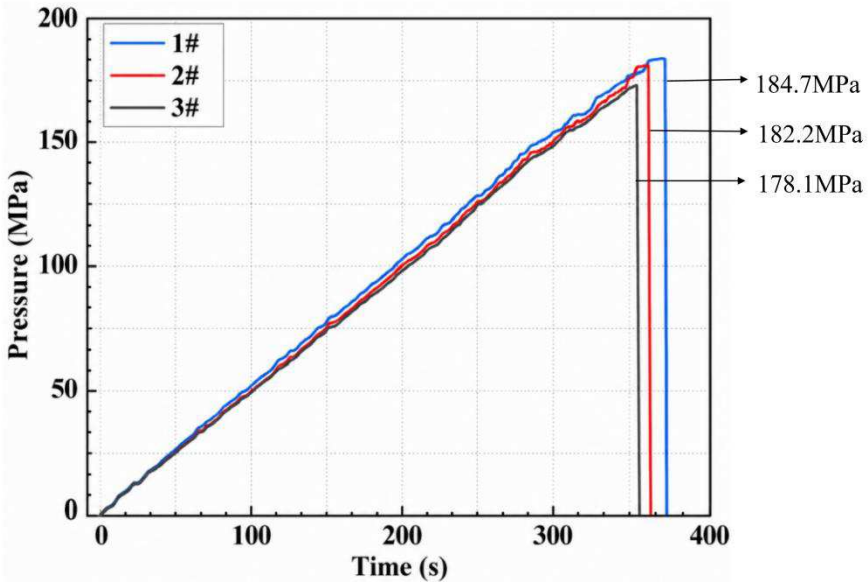


Fig. 11 Burst-pressure curves for composite pressure vessels 1# – 3#

To validate the proposed model, burst tests were performed on three composite pressure vessels, and the experimental results are summarized in Table 6. To ensure the reliability of the data, the mean and standard deviation (SD) of the burst pressures for the three specimens were calculated. The standard deviation quantifies the dispersion among the three measurements, with a smaller value indicating greater consistency. The measured burst pressures were relatively consistent, yielding an average value of 181.7 MPa. The finite element analysis (FEA) prediction of 189.0 MPa differed from the experimental mean by only 4.0%, indicating good agreement between the numerical and experimental results. The close correspondence between the experimental and predicted burst pressures demonstrates that the finite element modeling approach developed in this study, together with the customized USDFLD subroutine based on the Hashin failure criterion, can accurately predict the burst performance of Type IV composite pressure vessels.

Table 6 Comparison of experimental and predicted burst pressures

Vessel	Experimental burst pressure (MPa)	Predicted burst pressure (MPa)	Relative deviation (%)
1#	184.7	189.0	4.0%
2#	182.2		
3#	178.1		
Mean ± SD	181.7±2.7		

As illustrated in Figure 12, all three composite pressure vessels exhibited extensive fragmentation in

the cylindrical section under hydrostatic loading. This failure pattern was consistent with the finite element predictions, and distinct ruptures were also observed at the dome – cylinder transition regions.

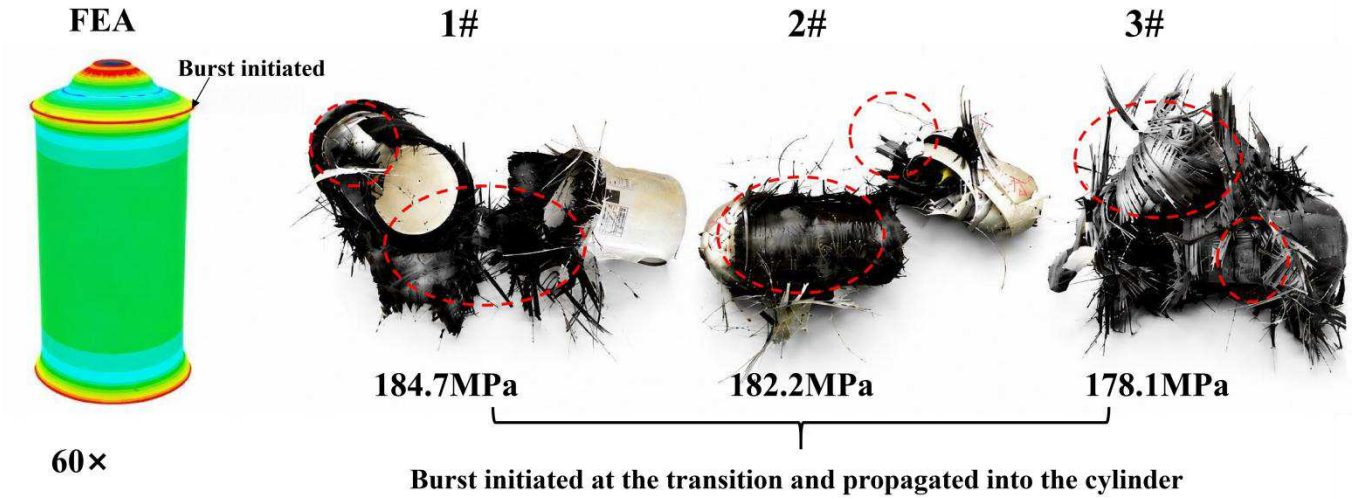


Fig. 12 Burst failure modes of the composite pressure vessels

5. Conclusions

This study clarified the relationship between process-induced winding geometry, progressive damage evolution, and failure localization in dry-towpreg-wound 70 MPa Type IV hydrogen vessels. Spatial variations in winding angle and thickness, together with curvature variations and stiffness mismatch among the aluminum boss, PA6 liner, and composite overwrap, produced local stress concentrations near the polar boss and the dome – cylinder transition. Matrix tensile damage therefore initiated at approximately 32 MPa in these regions. As the pressure increased, matrix damage reduced the local stiffness and redistributed the load to the surrounding composite layers. The damaged region then extended from the domes and transition zones toward the cylindrical section.

The failure process changed from early matrix-dominated damage to extensive fiber tensile damage in the primary load-bearing layers. Compressive damage remained limited because internal pressure mainly generated tensile stresses in the fiber and transverse directions. At the final numerical stage of 189 MPa, the predicted damaged-volume fractions for matrix tension and fiber tension were approximately 79.2% and 51.8%, respectively. These values describe the damage state of the present model and do not represent

universal burst thresholds. The marked pressure–displacement nonlinearity above approximately 165 MPa indicated that distributed material damage had caused a substantial loss of structural stiffness.

The dome–cylinder transition exhibited the largest deformation and the strongest damage localization. This critical response resulted from the combined effects of geometric discontinuity, local thickness build-up, winding-angle variation, and material stiffness mismatch. Extensive stiffness degradation caused numerical loss of convergence at 189.0 MPa, which was taken as the predicted burst pressure. The experimental mean burst pressure was 181.7 ± 2.7 MPa, corresponding to a relative deviation of 4.0%. Post-burst fragmentation across the transition and the adjacent cylindrical section was spatially consistent with the predicted critical region. These results reveal a progressive failure path from geometry-induced stress concentration to matrix damage, fiber damage accumulation, structural stiffness loss, and localized burst failure. This mechanism provides a basis for prioritizing the dome–cylinder transition and polar-boss regions in subsequent structural design. Future studies should consider manufacturing variability and additional vessel configurations.

Acknowledgments

This work was supported by the Hebei Province Central Guidance Fund for Local Science and Technology Development Project (No. 246Z0202G);the Central Guidance Fund for Local Science and Technology Development in Hebei Province, No. 264Z1405G, the Science Research Project of the Hebei Education Department (No. BJK2023002); the Research Project of Science and Technology for Higher Education Institutions in Hebei Province (No. QN2024073); and the Research Fund of the North China Institute of Aerospace Engineering (No. KY-2024-02).

Competing Interests

The authors declare that they have no known competing financial interests or personal relationships that could have appeared to influence the work reported in this paper.

Data Availability

Data will be made available on request.

References

[1] Shiraishi, K., Park, W., Kammen, D.M.: The role of hydrogen as long-duration energy storage and as an international energy carrier for electricity sector decarbonization. Environ. Res. Lett. 19, 084011 (2024). https://doi.org/10.1088/1748-9326/ad5856

[2] Zhang, Q., Xu, H., Jia, X., Zu, L., Cheng, S., Wang, H.: Design of a 70 MPa type IV hydrogen storage vessel using accurate modeling techniques for dome thickness prediction. Compos. Struct. 236, 111915 (2020). https://doi.org/10.1016/j.compstruct.2020.111915

[3] Liu, H., Xu, L., Han, Y., Chen, X., Sheng, P., Wang, S., Huang, X., Wang, X., Lu, C., Luo, H., He, S., Lan, Z., Guo, J.: Development of a gaseous and solid-state hybrid system for stationary hydrogen energy storage. Green Energy Environ. 6, 528–537 (2021). https://doi.org/10.1016/j.gee.2020.06.006

[4] Adams, J., Houchins, C., Ahluwalia, R.: Onboard Type IV Compressed Hydrogen Storage System—Cost and Performance Status. DOE Hydrogen and Fuel Cells Program Record 19008, U.S. Department of Energy (2019)

[5] International Organization for Standardization: ISO 19881:2025, Gaseous hydrogen—Land vehicle fuel containers. ISO, Geneva (2025)

[6] SAE International: SAE J2579_202301, Standard for Fuel Systems in Fuel Cell and Other Hydrogen Vehicles. SAE International, Warrendale (2023). https://doi.org/10.4271/J2579_202301

[7] Jois, K.C., Welsh, M., Gries, T., Sackmann, J.: Numerical analysis of filament wound cylindrical composite pressure vessels accounting for variable dome contour. J. Compos. Sci. 5, 56 (2021). https://doi.org/10.3390/jcs5020056

[8] Regassa, Y., Gari, J., Lemu, H.G.: Composite overwrapped pressure vessel design optimization using numerical method. J. Compos. Sci. 6, 229 (2022). https://doi.org/10.3390/jcs6080229

[9] Dai, B., Zhou, M., Zhang, J., Li, Y., Jin, W.: Optimization design of filament wound composite pressure

vessel based on OpenSees. Appl. Sci. 13, 4894 (2023). https://doi.org/10.3390/app13084894

[10] Bouhala, L., Karatrantos, A.V., Reinhardt, H., Schramm, N., Akin, B., Rauscher, A., Mauersberger, A., Taşkıran, S.T., Ulaşlı, M.E., Aktaş, E., Tanoğlu, M.: Advancement in the modeling and design of composite pressure vessels for hydrogen storage: a comprehensive review. J. Compos. Sci. 8, 339 (2024). https://doi.org/10.3390/jcs8090339

[11] Mikroni, M., Koutsoukis, G., Vlachos, D., Kostopoulos, V., Vavouliotis, A., Trakakis, G., Athinaios, D., Nikolakea, C., Zacharakis, D.: Design, analysis, and testing of a Type V composite pressure vessel for hydrogen storage. Polymers 16, 3576 (2024). https://doi.org/10.3390/polym16243576

[12] Fei, J., Yang, C., Song, Y.: Review on strength failure criteria of anisotropic composite materials. Chin. J. Theor. Appl. Mech. 56, 1006 – 1024 (2024). https://doi.org/10.6052/0459-1879-23-507

[13] Millen, S.L.J., Aravand, M.A.: Assessing the relative conservatism of the unit circle failure envelope. Compos. Commun. 24, 100690 (2021). https://doi.org/10.1016/j.coco.2021.100690

[14] Tsai, S.W., Wu, E.M.: A general theory of strength for anisotropic materials. J. Compos. Mater. 5, 58 – 80 (1971). https://doi.org/10.1177/002199837100500106

[15] Kaddour, A.S., Hinton, M.J.: Maturity of 3D failure criteria for fibre-reinforced composites: comparison between theories and experiments: Part B of WWFE-II. J. Compos. Mater. 47, 925 – 966 (2013). https://doi.org/10.1177/0021998313478710

[16] Kassa, M.K., Selvaraj, R., Arumugam, A.B.: A finite element based progressive failure analysis of carbon nanotubes/polymer/fiber reinforced laminated composite tapered panels. Fibers Polym. 23, 3552 – 3568 (2022). https://doi.org/10.1007/s12221-022-4072-9

[17] Kurkaani Barvaj, A., Ghannadpour, S.A.M., Nafar Dastgerdi, J., Ovesy, H.R.: Finite strip progressive damage analysis of relatively thick imperfect laminates under end-shortening strain. Acta Mech. 234, 5229 – 5248 (2023). https://doi.org/10.1007/s00707-023-03656-6

[18] Patel, M., Sonkar, L., Patel, S.: Assessment of ply stacking sequence effect on damage behavior of

CFRP composite laminate under low-velocity impacts. Adv. Mater. Sci. Eng. 2025, 4349535 (2025). https://doi.org/10.1155/amse/4349535

[19] Liu, Y., Xie, J., Chen, X., Zhang, J., Wan, M., Sun, Z., Yang, C.: Characterization of progressive damage behaviour and failure mechanism of carbon fiber reinforced composite laminates. Sci. Rep. 15, 13791 (2025). https://doi.org/10.1038/s41598-025-98774-7

[20] Xu, J., Xu, Y., Gu, Y., Zhang, X., Zhang, H.: Research on preprocessing of winding trajectory of composite type IV pressure vessel based on robot. J. Mech. Sci. Technol. 36, 5995 – 6004 (2022). https://doi.org/10.1007/s12206-022-1115-5

[21] Wang, T., Ge, P., Gao, D., Gao, G., Qi, T.: Winding pattern design for composite pressure vessels based on fiber overlap and stacking optimization. J. Compos. Mater. 60, 1199 – 1216 (2026). https://doi.org/10.1177/00219983251379937

[22] Wang, L., Zheng, C., Luo, H., Wei, S., Wei, Z.: Continuum damage modeling and progressive failure analysis of carbon fiber/epoxy composite pressure vessel. Compos. Struct. 134, 475 – 482 (2015). https://doi.org/10.1016/j.compstruct.2015.08.107

[23] Liang, J., Xue, Y., Li, Y., Zhao, C., Liu, J., Zhao, X., Zu, L.: Design of continuous transition line pattern between layers of composite pressure vessel. J. Reinf. Plast. Compos. 44, 620 – 633 (2025). https://doi.org/10.1177/07316844241226548

[24] Nie, X., Nan, B.: Ply-overlap fiber reinforced plastic connection structure design and discrete optimization. J. Mech. Eng. 57, 194 – 203 (2021). https://doi.org/10.3901/JME.2021.07.194

[25] Wang, H., Fu, S., Chen, Y., Hua, L.: Thickness-prediction method involving tow redistribution for the dome of composite hydrogen storage vessels. Polymers 14, 902 (2022). https://doi.org/10.3390/polym14050902

[26] Li, J., Zhao, C., Gao, J., Guo, H.: Study on structural design and stress simulation of carbon fiber composite Type IV hydrogen storage cylinder. Sci. Rep. 16, 22960 (2026).

https://doi.org/10.1038/s41598-025-18865-3

[27] Okten, Y.K., Kaynak, C.: Mechanical performance of composite flat specimens and pressure vessels produced by carbon/epoxy towpreg dry winding. J. Reinf. Plast. Compos. 42, 558 – 576 (2023). https://doi.org/10.1177/07316844221134029

[28] Ueda, M., Hidaka, T., Ichihara, N., Yang, H., Iwase, W., Matsuda, T., Morita, N., Aoki, R., Yokozeki, T.: Voids in type-IV composite pressure vessels manufactured by a dry filament-winding process. Int. J. Press. Vessels Pip. 208, 105154 (2024). https://doi.org/10.1016/j.ijpvp.2024.105154

[29] Reda, R., Habib, E.-S.: Manufacturing challenges of Type IV hydrogen composite vessels: computational – experimental divergence in emerging resource-constrained economies. J. Eng. Appl. Sci. 73, 156 (2026). https://doi.org/10.1186/s44147-026-01010-w

[30] Hur, J.R., Hoover, D., Ballard, K., Varshney, V., Przybyla, C.P., Kalidindi, S.R.: Computational protocols for the study of damage initiation in unidirectional fiber-reinforced polymer matrix composites. Integr. Mater. Manuf. Innov. 14, 714 – 726 (2025). https://doi.org/10.1007/s40192-025-00429-y

[31] Wu, X., Yang, B., Zhou, S.: Strength and failure analysis of fiber-wound composite gas cylinder via numerical simulation. Materials 17, 717 (2024). https://doi.org/10.3390/ma17030717

[32] Hashin, Z.: Failure criteria for unidirectional fiber composites. J. Appl. Mech. 47, 329 – 334 (1980). https://doi.org/10.1115/1.3153664

[33] Zhou, W., Wang, J., Pan, Z., Liu, J., Ma, L., Zhou, J., Su, Y.: Review on optimization design, failure analysis and non-destructive testing of composite hydrogen storage vessel. Int. J. Hydrog. Energy 47, 38862 – 38883 (2022). https://doi.org/10.1016/j.ijhydene.2022.09.028

[34] Lin, J., Zheng, C., Dai, Y., Wang, Z., Lu, J.: Prediction of composite pressure vessel dome contour and strength analysis based on a new fiber thickness calculation method. Compos. Struct. 306, 116590 (2023). https://doi.org/10.1016/j.compstruct.2022.116590

[35] Mehrabianbardar, A., Shirinbayan, M., Jendli, Z., Gillet, S., Nouira, S., Fitoussi, J.: A review:

challenges, processes, and innovations in high-pressure hydrogen storage technologies. Int. J. Mater. Form. 18, 77 (2025). https://doi.org/10.1007/s12289-025-01934-3

[36] Jin, S., Cheng, P., Bai, Y., Paik, J.K., Li, J.: Progressive failure analysis and burst mode study of type IV composite vessels. Ships Offshore Struct. (2022). https://doi.org/10.1080/17445302.2022.2157192